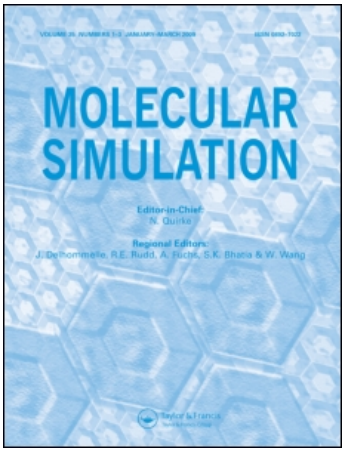

Molecular Simulation
Publication details, including instructions for authors and subscription information:
http://www.informaworld.com/smpp/title~content=t713644482

An ultrathin carbon nanoribbon study as a component of nanoelectromechanical devices

J. W. Kang[a]; H. J. Hwang[a]
[a] Nano Electronics Future Technology Laboratory, School of Electrical and Electronic Engineering, Chung-Ang University, DongJak-Ku, Seoul, South Korea

To cite this Article Kang, J. W. and Hwang, H. J.(2005) 'An ultrathin carbon nanoribbon study as a component of nanoelectromechanical devices', Molecular Simulation, 31: 8, 561 — 565
To link to this Article: DOI: 10.1080/08927020500044954
URL: http://dx.doi.org/10.1080/08927020500044954

Molecular Simulation, Vol. 31, No. 8, July 2005, 561–565

Taylor & Francis
Taylor & Francis Group

An ultrathin carbon nanoribbon study as a component of nanoelectromechanical devices

J. W. KANG* and H. J. HWANG

Nano Electronics Future Technology Laboratory, School of Electrical and Electronic Engineering, Chung-Ang University, 221 HukSuk-Dong, DongJak-Ku, Seoul 156-756, South Korea

(Received December 2004; in final form January 2005)

We investigated a carbon nanoribbon (CNR) using atomistic simulations based on Tersoff–Brenner potential function. The CNR was obtained from a compressed (5,5) carbon nanotube (CNT). The obtained CNR had a cross-sectional view as a binocular telescope structure composed of both sp^2 and sp^3 bonds. One carbon atom per ten carbon atoms had sp^3 bond. For the optimized structures, the residual forces on the CNR were 3-order higher than that on the CNR and the lattice constant of the CNR was higher 0.0624 Å than that of the CNT along the tube axis. The Young's modulus of the CNR was the same as that of the CNT whereas the critical strain of the CNR was significantly lower than that of the CNT because the residual stresses on the CNR was very higher than those on the CNT. The tensile force curve vs. the strain of the CNT was slightly higher than that of the CNR.

Keywords: Carbon Nanoribbon; Carbon Nanotube; Nanoelectromechanical Deivce; Atomistic Simulation; Molecular Dynamics

1. Introduction

Carbon nanotubes (CNT) [1] are excellent candidates for nanoelectromechanical system (NEMS) devices not only because of their excellent electronic and mechanical properties, but also because of the significant progress that have been made in the last few years in fabrication of carbon nanostructures [2]. Since CNTs have well-characterized chemical and physical structures, low mass and dimensions, exceptional directional stiffness, and range of electronic properties [3], various prototypes CNT-based NEMS have already been demonstrated, such as gigahertz oscillators [4–9], data storage nanodevices [10–13], nanotransport channels [14], sensors [15] and nanorelay [16–21].

Lee *et al.* [21] fabricated the CNT nanorelay devices, which are acted as a switch in the GHz regime and to be potentially suitable for applications such as logic devices, memory elements, pulse generators and current or voltage amplifiers [18]. Nantero Inc. [22] presented the electro-mechanical memory array using carbon nanoribbon (CNR). This nanotube random access memory (NRAM) is composed of the CNRs, freely suspended between source and drain electrodes, in the vicinity of a gate. Dequesnes *et al.* [16] theoretically investigated the NEM switch based on the CNT-bridge. Sapmaz *et al.* [23] have theoretically investigated in interplay between electrical and mechanical properties of NEM switch based on the CNT-bridge. Sazonova *et al.* [24] fabricated the tunable NEM CNT oscillator. CNT-bridges were suspended over a trench between both metal electrodes. The three-terminal device consists of a conducting CNT-bridge placed on the trenched substrate and connected to the fixed source and drain electrodes. A gate electrode is positioned underneath the CNT-bridge so that charge can be induced in the CNT-bridge by applying a gate voltage. The resulting capacitive force between the CNT-bridge and the gate bends the CNT-bridge and brings the CNT-bridge into contact with the substrate.

The structure of the NRAM can be fabricated by the contemporary silicon technologies [22]. The key components are a movable CNR as switching bridge and a gate electrode for position control of the movable CNR. When the potential different is achieved between the CNR and the gate electrode, electrical charges are induced on both the CNR and the gate electrode. Electrical charges induced on the suspended CNR give rise to electrostatic force, which deflect the CNR. The resulting capacitive force between the CNR and the gate bends the CNR and brings the CNR into the van der Waals (vdW) contact with

*Corresponding author. Tel.: +82-2-820-5296. Fax: +82-2-825-1584. E-mail: gardenriver@korea.com

Molecular Simulation
ISSN 0892-7022 print/ISSN 1029-0435 online © 2005 Taylor & Francis Ltd
http://www.tandf.co.uk/journals
DOI: 10.1080/08927020500044954

the gate electrode. In addition to electrostatic forces, depending on the gap between the CNR and the gate electrode, the vdW interactions also act on the CNR and deflect the CNR. The electrostatic and the vdW forces make the CNR to bend toward the gate electrode. Counteracting the electrostatic and the vdW forces are elastic forces, which try to restore the CNR to its original straight position. For an applied voltage, an equilibrium position of the CNR is obtained from the balance of the elastostatic, the electrostatic, and the vdW forces. When the applied potential difference between the CNR and the gate electrode exceeds a certain potential, the CNR becomes unstable and contacts onto the gate electrode. The potential difference, which causes the CNR to contact onto the gate electrode, is defined as the pull-in voltage. When the pull-in voltage is applied, the CNT-ribbon comes in contact with the gate electrode, and the device is said to be in the ON state. When the potential is released and the CNR and the gate electrode are separated, the device is said to be in the OFF state. Due to the exponential dependence of the tunneling resistance on CNR deflection, there is a sharp transition from OFF to ON states when the gate voltage is varied at fixed source-drain voltage. The sharp switching curve allows for amplification of weak signals superimposed on the gate voltage.

The structural and the mechanical properties of the CNTs including the oscillation of the CNTs have been extensively investigated using experimental and theoretical studies. However, CNRs have not been investigated until now. In this paper, we investigate a CNR suspended with both rigid edges using atomistic simulations and compare CNR to CNT in the structural and the mechanical properties.

2. Simulation methods

For carbon-carbon interactions, we used the Tersoff–Brenner potential function that has been widely applied to carbon systems [25–27]. We used both steepest descent (SD) and molecular dynamics (MD) methods. The MD simulations used the same MD methods as were used in our previous works [28–31]. The MD code used the velocity Verlet algorithm, a Gunsteren–Berendsen thermostat to control temperature, and neighbor lists to improve computing performance [32]. The MD time step was 5×10^{-4} ps. Initial velocities were assigned from the Maxwell distribution and the magnitudes were adjusted so as to keep the temperature in the system. The boundary atoms of the CNT or the CNR were fixed in the SD and MD simulations and the other atoms were applied to free SD and MD simulations.

In this work, the external force per atom (F_{appl}) was considered as the electrostatic force on carbon atom induced by the gate voltage. We assumed that the gate electrode was infinitely separated with the CNR or CNT; then, the potential along the CNR or the CNT was assumed as constant. Therefore, the same electrostatic force was applied to carbon atoms composed of the CNT or the CNR.

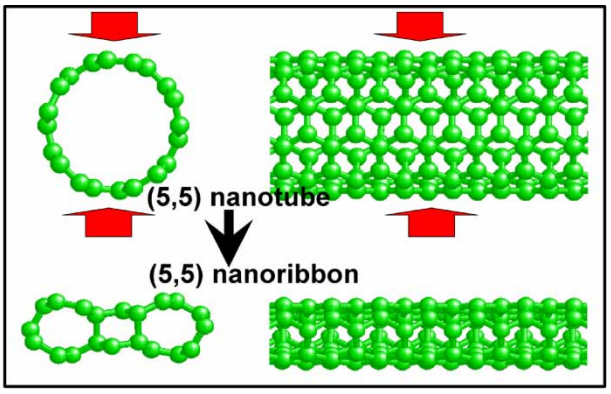

Figure 1. Atomic structure for the (5,5) CNT and the (5,5) CNR in this study.

3. Results and discussion

3.1 A CNR structure

Figure 1 shows the atomic structure for the (5,5) CNT and the (5,5) CNR in this study. The length of the (5,5) CNT was 116.826 Å. The numbers of carbon atoms composed of the CNT and the CNR were 960. To obtain the CNR from the (5,5) CNT, we assumed that the (5,5) CNT was intercalated between the infinite rigid sheets. The interaction between the CNT and the sheets was temporary modeled by the Lennard–Jones 12–6 potential function with the parameters $\varepsilon = 1$ eV and $\sigma = 4$ Å. The distance between both the sheets (d_{ss}) was decreased from 30 to 12 Å with 0.2 Å per 10^4 SD steps. Figure 2(a) shows the potential energy per atom as a function of d_{ss}. When $d_{\text{ss}} > 20$ Å, the CNT was not compressed and the potential was constant. When $14.4\,\text{Å} < d_{\text{ss}} < 20\,\text{Å}$, the CNT was compressed; then, the potential energy was increased. When $d_{\text{ss}} = 14.2$ Å, the

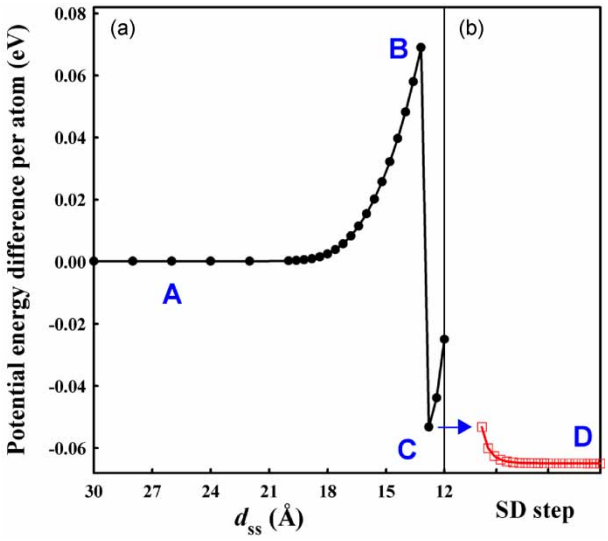

Figure 2. (a) Potential energy per atom as a function of d_{ss}. (b) Potential energy per atom as a function of SD step when the SD simulation without the both sheets was performed using the atomic structure of the label C. The atomic structures corresponding the labels A, B, C, and D can be found in Figs. 1, 3 and 4.

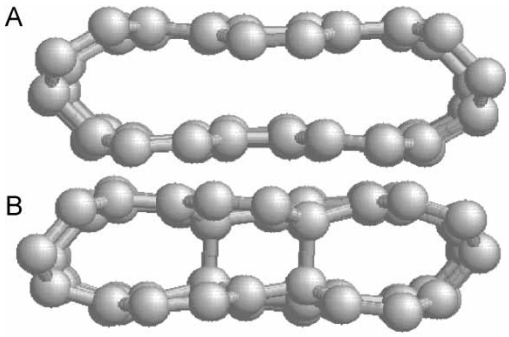

Figure 3. Atomic structures corresponding to the labels B and C in figure 2.

CNT was changed into the CNR structure with sp^3 hybridization; then, the potential energy was abruptly decreased. As d_{ss} decreased more and more, the potential energy was increased. Atomic structures corresponding to the labels A and D in figure 2 are presented in figures 1 and 4. Atomic structures corresponding to the labels B and C in figure 2 are presented in figure 3. With the atomic structure of the label C with the lowest energy, we performed the SD simulation without the both sheets as shown in figure 2(b). At the C point, one carbon atom per ten carbon atoms has sp^3 bond. Finally, the CNR had a cross-sectional view as a binocular telescope structure with two tube composed of only sp^2 bonds and a core composed of sp^3 bond as shown in figures 1 and 4. For various nanotubes, the strain energy increases with the decreasing of the radius of the nanotube [33–36]. Therefore, it is clear that the strain energy and the residual stress for the CNR structure as shown in figures 1 and 4 are higher than those for the CNT structure. This means that the residual forces on the CNR are higher than that on the CNT. Figure 4 shows the residual forces on both the optimized CNT and CNR. The residual forces on the optimized CNT are very low whereas the residual forces on the optimized CNR are above 3-order higher than those on the optimized CNT. The length of the (5,5) CNR obtained from this work was 119.821 Å; then, the lattice constant of the CNR is higher 0.0624 Å than that of the CNT along the tube axis.

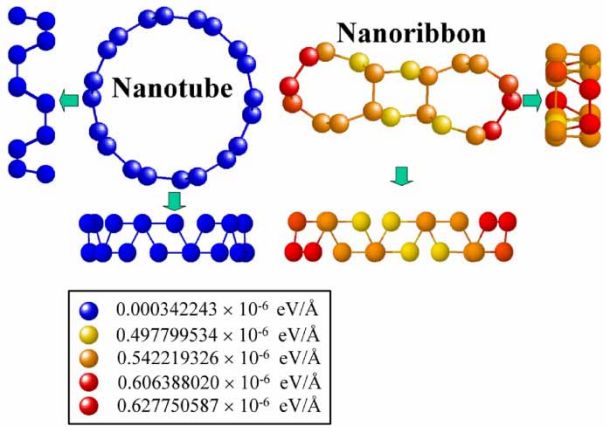

Figure 4. The residual forces on both the CNT and the CNR.

3.2 Mechanical properties of the CNR

Since we used the optimized CNT and CNR in our study, there was no slack in the suspended the CNT and CNR. Figure 5 shows the results of the tensile testing of the CNT and the CNR below the critical points. Figure 5(a), (b) show the strain energy and the tensile force as a function of the strain. In figure 5(a), the strain energy curve vs. the strain of the CNT is in agreement with that of the CNR. Therefore, the Young's modulus of the CNR is the same as that of the CNT. It is clear that during the stretching of the CNT, the strain energy increasing is induced by only extension of the sp^2 bond lengths. Therefore, the results in figure 5(a) imply that during the CNR stretching, the strain energy increasing of the atom with sp^3 bond is similar to that with sp^2 bond.

However, in figure 5(a), the tensile force curve vs. strain of the CNT is slightly higher than that of the CNR. This reason can be explained that the cross-sectional area of the CNR is lower than that of the CNT. Also, as discussed in figure 4, the residual stresses on the CNR make that the tension of the CNR is slightly lower than the tension of the CNT for the same strain; the, the critical strain of the CNR is significantly lower than that

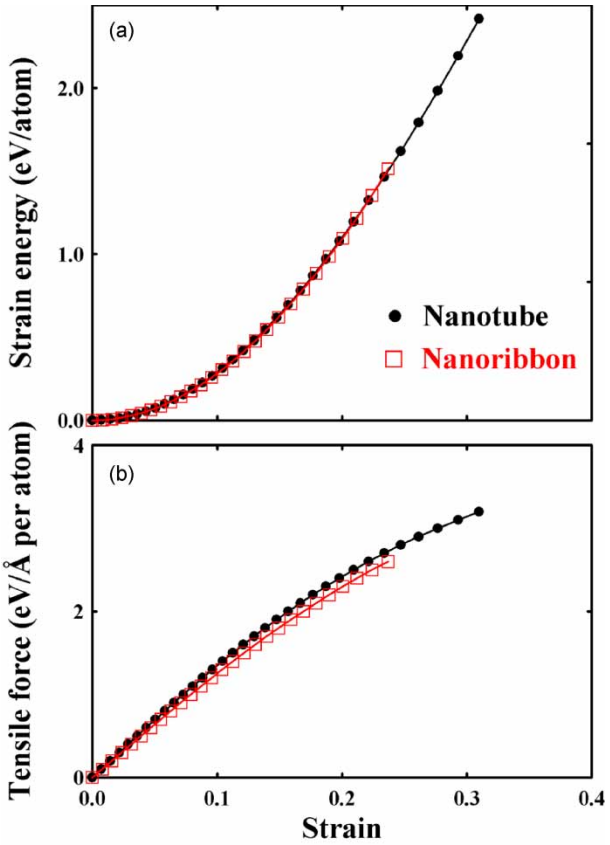

Figure 5. Results of the tensile testing of the CNT and the CNR below the critical points. (a) and (b) show the strain energy and the tensile force as a function of the strain.

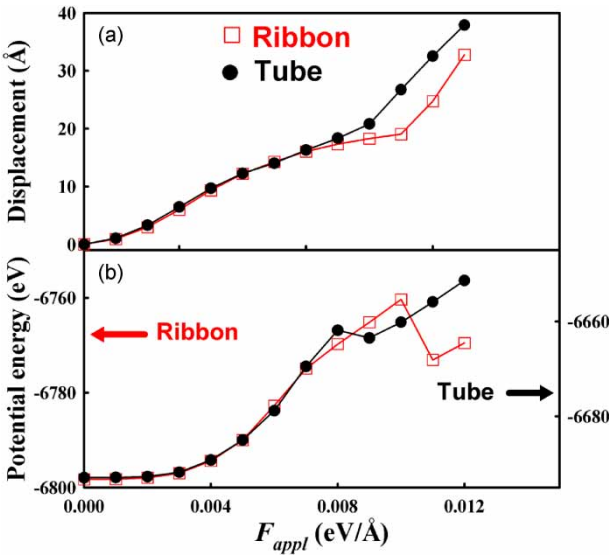

Figure 6. Displacement and potential energy variations of the bridges as a function of the F_{appl}.

of the CNT. This implies that the electromechanical operation of the NRAM based on CNRs is different from that based on CNTs. Therefore, the further study on the CNRs should be performed.

We performed the SD simulations for the CNR and the CNT bending in the conditions that both edges were fixed. The external forces per atom (F_{appl}) applied to the suspended CNR and CNT were perpendicular to their axis's. Figure 6 show the displacement and the potential energy variations of the bridges as a function of the F_{appl}. The displacements in figure 6(a) were calculated the displacement of the center of the CNT and the CNR along the direction of the F_{appl}. Below the critical point of the CNR, the displacements and the potential energy variations of both the CNR and the CNT are the same. The atomic bond breakings for the CNR and the CNT were achieved from $F_{\text{appl}} = 0.008$ and $0.009\,\text{eV/Å}$, respectively. For the CNR case, just one atomic bond was broken when the $F_{\text{appl}} = 0.008\,\text{eV/Å}$ and the CNR was maintained until $F_{\text{appl}} = 0.01\,\text{eV/Å}$; then, the CNR was broken when the $F_{\text{appl}} = 0.011\,\text{eV/Å}$. However, for the CNT case, the CNT was abruptly broken when the $F_{\text{appl}} = 0.009\,\text{eV/Å}$. This reason can be explained as follows; (i) although the critical strain of the CNR is lower than that of the CNT, the total potential energy of the CNR is lower than that of the

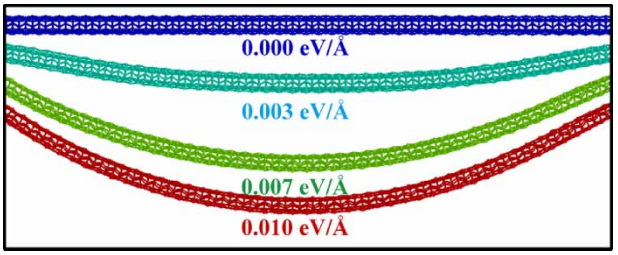

Figure 7. Atomic structures of the CNR when the $F_{\text{appl}} = 0$, 0.003, 0.007, and 0.01 eV/Å.

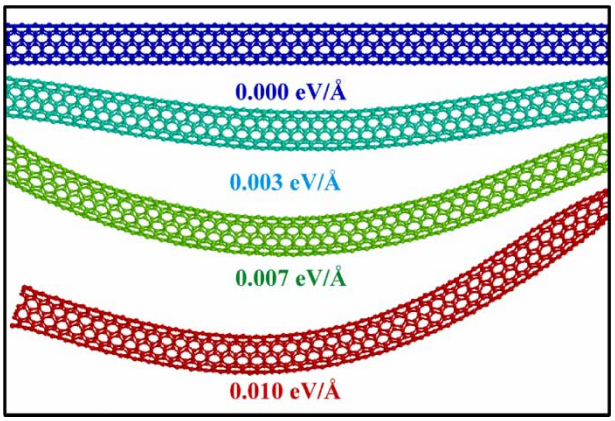

Figure 8. Atomic structures of the CNT when the $F_{\text{appl}} = 0$, 0.003, 0.007, and 0.01 eV/Å.

CNT; i.e. the atomic binding energy of the CNR is higher than that of the CNT and (ii) the ribbon-like structure is more flexible than the tubular structure in their bending cases. The atomic structures of the CNR and the CNT under the F_{appl} are shown in figures 7 and 8, respectively.

Figure 9 shows the results of the MD simulations for the suspended CNR and CNT when the $F_{\text{appl}} = 0.003\,\text{eV/Å}$. Figure 9(a), (b) show the displacement and the potential energy variation as a function of the MD time, respectively. The center of the displacement for both cases is 6 Å, which is in excellent agreement with the results obtained from the SD simulations as shown in figure 6(a). The oscillation frequency of the CNT, 83.5 GHz, is slightly higher than that of the CNR, 81.7 GHz. This result is explained that the tubular structure is more rigid than the ribbon-like structure in their bending cases. The difference in the oscillation frequencies of the CNR and the CNT can make the difference in the data

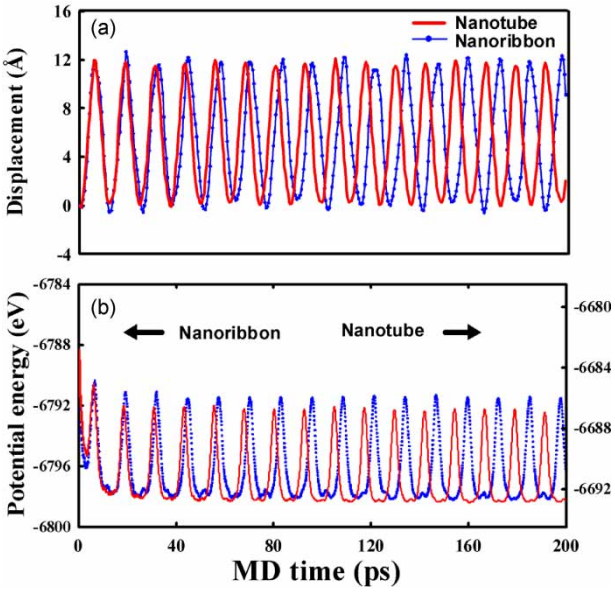

Figure 9. Results of the MD simulations for the CNR- and the CNT-bridges when the $F_{\text{appl}} = 0.003\,\text{eV/Å}$. (a) and (b) show the displacement and the potential energy variation as a function of the MD time, respectively.

throughput rate of the NRAM. Therefore, this relation should be investigated in further works.

4. Summary

We investigated a CNR, which was obtained from a compressed (5,5) CNT, using atomistic simulations based on Tersoff–Brenner potential function. The obtained CNR had a cross-sectional view as a binocular telescope structure with two tube composed of sp^2 and sp^3 bonds. One carbon atom per ten carbon atoms had sp^3 bond. The residual forces on the CNR were 3-order higher than that on the CNR. The lattice constant of the CNR was higher 0.0624 Å than that of the CNT along the tube axis. The Young's modulus of the CNR was the same as that of the CNT whereas the critical strain of the CNR was significantly lower than that of the CNT because the residual stresses on the CNR was very higher than those on the CNT. The tensile force curve vs. the strain of the CNT was slightly higher than that of the CNR. These results implied that the electromechanical operations of the NRAM based on CNRs were different from that based on CNTs.

References

[1] S. Iijima. Helical microtubules of graphitic carbon. *Nature*, **354**, 56 (1991).

[2] W.A. Goddard, D.W. Brenner, S.E. Lyshevski, G.J. Iagrate (Eds.). *Handbook of Nanoscience, Engineering, and Technology*, CRC Press, New York (2003).

[3] D. Dian, G.J. Wagner, W.K. Liu, M.-Y. Yu, R.S. Ruoff. Mechanics of carbon nanotubes. *Appl. Mech. Rev.*, **55**, 495 (2002).

[4] Q. Zheng, Q. Jiang. Multiwalled carbon nanotubes as gigahertz oscillators. *Phys. Rev. Lett.*, **88**, 045503 (2002).

[5] Q. Zheng, J.S. Liu, Q. Jiang. Excess van der Waals interaction energy of a multiwalled carbon nanotube with an extruded core and the induced core oscillation. *Phys. Rev. B*, **65**, 245409 (2002).

[6] Y. Zhao, C.-C. Ma, G.H. Chen, Q. Jiang. Energy dissipation mechanisms in carbon nanotube oscillators. *Phys. Rev. Lett.*, **91**, 175504 (2003).

[7] S.B. Legoas, V.R. Coluci, S.F. Braga, P.Z. Coura, S.O. Dantas, D.S. Galvao. Molecular-dynamics simulations of carbon nanotubes as Gigahertz oscillators. *Phys. Rev. Lett.*, **90**, 055504 (2003).

[8] S.B. Legoas, V.R. Coluci, S.F. Braga, P.Z. Coura, S.O. Dantas, D.S. Galvao. Gigahertz nanomechanical oscillators based on carbon nanotubes. *Nanotechnology*, **15**, S184 (2004).

[9] J.W. Kang, H.J. Hwang. Gigahertz actuator of multiwall carbon nanotube encapsulating metallic ions: molecular dynamics simulations. *J. Appl. Phys.*, **96**, 3900 (2004).

[10] W.Y. Choi, J.W. Kang, H.J. Hwang. Bucky shuttle memory system based on boron-nitride nanopeapod. *Physica E*, **23**, 135 (2004).

[11] J.W. Kang, H.J. Hwang. Carbon nanotube shuttle memory device. *Carbon*, **42**, 3018 (2004).

[12] J.W. Kang, H.J. Hwang. Schematics and atomistic simulations of nanomemory element based on carbon tube-to-peapod transition. *Jpn. J. Appl. Phys.*, **73**, 4447 (2004).

[13] T. Rueckes, K. Kim, E. Joselevich, G.Y. Tseng, C.-L. Cheung, C.M. Liever. Reversible, bistable carbon nanotube devices for molecular computing. *Science*, **289**, 94 (2000).

[14] M.W. Roth, J. Mesentseva. Atomistic simulations of rare gas transport through breathable single-wall nanotubes with constrictions and knees. *Mol. Simul.*, **30**, 661 (2004).

[15] P.G. Collins, K.B. Bradley, M. Ishigamo, A. Zettl. Extreme oxygen sensitivity of electronic properties of carbon nanotubes. *Science*, **287**, 1801 (2000).

[16] M. Dequesnes, S.V. Rotkin, N.R. Aluru. Calculation of pull-in voltages for carbonnanotube-based nanoelectromechanical switches. *Nanotechnology*, **13**, 120 (2002).

[17] J.M. Kinaret, T. Nord, S. Viefers. A carbon-nanotube-based nanorelay. *Appl. Phys. Lett.*, **82**, 1287 (2003).

[18] C. Ke, H.D. Espinosa. Feedback controlled nanocantilever device. *Appl. Phys. Lett.*, **85**, 681 (2004).

[19] L.M. Jonsson, T. Nord, J.M. Kinaret, S. Viefers. Effects of surface forces and phonon dissipation in a three-terminal nanorelay. *J. Appl. Phys.*, **96**, 629 (2004).

[20] L.M. Jonsson, S. Axelsson, T. Nord, S. Viefers, J.M. Kinaret. High frequency properties of a CNT-based nanorelay. *Nanotechnology*, **15**, 1497 (2004).

[21] S.W. Lee, D.S. Lee, R.E. Morjan, S.H. Jhang, M. Sveningsson, O.A. Nerushev, Y.W. Park, E.E.B. Campbell. A three-terminal carbon nanorelay. *Nano Lett.*, **4**, 2027 (2004).

[22] B.M. Segal, D.K. Block, R. Thomas. Electromechanical memory array using nanotube ribbons and method for making same, US Patent submission number 2004- 850100 (2004. 05. 20) (http://www.nantero.com).

[23] S. Sapmaz, Y.M. Blanter, L. Gurevich, H.S.J. van der Zant. Carbon nanotubes as nanoelectromechanical systems. *Phys. Rev. B*, **67**, 235414 (2003).

[24] V. Sazonova, Y. Yaish, H. Üstünel, D. Roundy, T.A. Arias, P.L. McEuen. A tunable carbon nanotube electromechanical oscillator. *Nature*, **431**, 284 (2004).

[25] J. Tersoff. Empirical interatomic potential for silicon with improved elastic properties. *Phys. Rev. B*, **38**, 9902 (1988).

[26] J. Tersoff. Modeling solid-state chemistry: Interatomic potentials for multicomponent systems. *Phys. Rev. B*, **39**, 5566 (1989).

[27] D.W. Brenner. Empirical potential for hydrocarbons for use in simulating the chemical vapor deposition of diamond films. *Phys. Rev. B*, **42**, 9458 (1990).

[28] M.P. Allen, D.J. Tildesley. *Computer Simulation of Liquids*, Clarendon Press, Oxford (1987).

[29] J.W. Kang, H.J. Hwang. Molecular dynamics simulations of single-wall GaN nanotubes. *Mol. Simul.*, **30**, 29 (2004).

[30] H.J. Hwang, K.R. Byun, J.W. Kang. Carbon nanotubes as nanopipette: modelling and simulations. *Physica E*, **23**, 208 (2004).

[31] J.W. Kang, H.J. Hwang. Fullerene nano ball bearings: Atomistic study. *Nanotechnology*, **15**, 614 (2004).

[32] J.W. Kang, H.J. Hwang. Comparison of C_{60} encapsulations into carbon and boron-nitride nanotubes. *J. Phys.: Condens. Matter*, **16**, 3901 (2004).

[33] O.A. Shenderova, D. Areshkin, D.W. Brenner. Bonding and stability of hybrid diamond/nanotube structures. *Mol. Simul.*, **29**, 259 (2003).

[34] P. Liu, Y.W. Zhang, H.P. Lee, C. Lu. Atomistic simulations of uniaxial tensile behaviors of single-walled carbon nanotubes. *Mol. Simul.*, **30**, 543 (2004).

[35] J.W. Kang, K.R. Byun, H.J. Hwang. Twist of hypothetical silicon nanotubes. *Model. Simul. Mater. Sci. Eng.*, **12**, 1 (2004).

[36] J.W. Kang, H.J. Hwang. An atomistic study on III-nitride nanotubes. *Comput. Mater. Sci.*, **31**, 237 (2004).